Clin Neuroradiol (2019) 29:177–184
https://doi.org/10.1007/s00062-019-00759-3

CLINICAL CASE

Freiburg Neuropathology Case Conference

Posterior Fossa Mass in an Infant

C. A. Taschner[1] · D. Erny[2] · M. J. Shah[3] · H. Urbach[1] · U. Feige[1] · M. Prinz[2]

Published online: 7 February 2019

Keywords Posterior fossa tumor · Infratentorial astrocytoma · Medulloblastoma · Atypical teratoid/rhabdoid tumor · Anaplastic ependymoma

Case Report

A 10-month-old boy became conspicuous 4–6 weeks before hospital admission with backward tilting of his head. He was finally admitted to hospital for decreased vigilance that had started 2 days prior to admission. Apart from anisocoric pupils the patient did not show any neurological deficits on admission. Magnetic resonance imaging (MRI) of the head showed an obstructive hydrocephalus in relation with a massive posterior fossa tumor. An external ventricular drainage was immediately placed. The subsequent craniotomy and operative excision of the tumor was performed with the patient in prone position. The tumor appeared cystic, with moderate bleeding and showed necrotic components. The tumor was resected down to the level of the fourth ventricle. Ventral to this level a separation from the cranial nerves and the brain stem was not possible, so that a significant amount of residual tumor remained. The postoperative course was uneventful. Apart from a slight strabismus there were no new postoperative neurological deficits. Due to a persisting hydrocephalus, a ventriculoperitoneal shunt was implanted 2 weeks later. The patient was discharged home 3 days after the second procedure.

✉ C. A. Taschner
christian.taschner@uniklinik-freiburg.de

[1] Department of Neuroradiology, Medical Centre—University of Freiburg, University of Freiburg, Breisacherstr. 64, 79106 Freiburg, Germany

[2] Department of Neuropathology, Medical Centre—University of Freiburg, University of Freiburg, Freiburg, Germany

[3] Department of Neurosurgery, Medical Centre—University of Freiburg, University of Freiburg, Freiburg, Germany

Imaging

The T2-weighted images showed a huge tumor mass located in the posterior fossa (Fig. 1a–c, arrow). The tumor displayed mixed signal intensities including hyperintense cystic components next to hypointense spotting, probably related to flow voids in the highly perfused tumor (Fig. 1b, *asterisk*). The lesion extended from the fourth ventricle into the prepontine and premedular cisterns (Fig. 1a–c, arrows), displacing the medulla oblongata (Fig. 1a, b, arrowhead), pons (Fig. 1c, arrowhead), mesencephalon and cerebellum. The tumor obstructed cerebrospinal fluid (CSF) circulation causing internal hydrocephalus (Fig. 1d, arrow) with transependymal leakage of CSF (Fig. 1d, arrowhead). On non-contrast T1-weighted images the tumor appeared less heterogeneous with isointense signal intensities when compared to the gray matter (Fig. 2a, arrow). On T1-weighted images after i.v. administration of gadolinium the tumor showd a moderate amount of regressive changes (Fig. 2b–d, arrowheads) with pronounced rim enhancement (Fig. 2b–d, arrow). On diffusion weighted images the tumor had an intermediate to high diffusion restriction (Fig. 3).

Differential Diagnosis

Infratentorial Astrocytoma

Cerebellar pilocytic astrocytoma (PA) is a benign tumor (World Health Organization, WHO grade I) and relatively uncommon in the first year of life. It is the most common pediatric central nervous system (CNS) tumor and the most frequent infratentorial tumor in the pediatric population [1]. Usually it appears as a cystic cerebellar mass hypointense or isointense in T1, hyperintense in T2 and

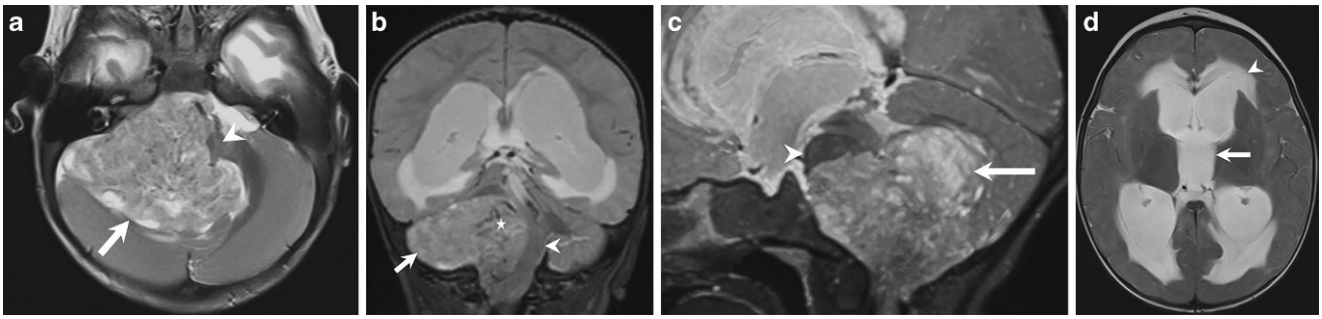

Fig. 1 Axial (**a**, **d**), coronal (**b**), and sagittal (**c**) T2-weighted images show a huge tumor mass located in the posterior fossa (**a**–**c**, *arrow*). The tumor displays mixed signal intensities including hyperintense cystic components next to hypointense spotting, probably related to flow voids in the highly perfused tumor (**b**, *asterisk*). The lesion extends from the fourth ventricle into the prepontine and premedular cisterns (**a**–**c**, *arrows*), displacing medulla oblongata (**a**, **b**, *arrowhead*), pons (**c**, *arrowhead*), mesencephalon, and cerebellum. The tumor obstructs cerebrospinal fluid (CSF) circulation causing internal hydrocephalus (**d**, *arrow*) with transependymal leakage of CSF (**d**, *arrowhead*)

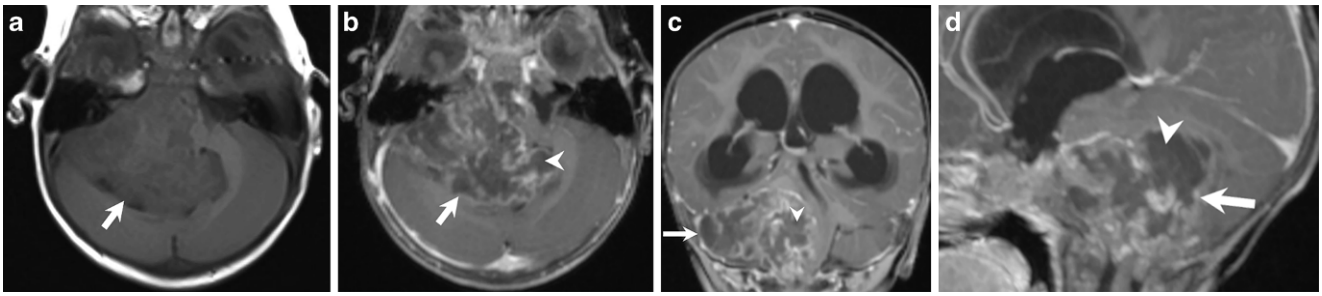

Fig. 2 On axial non-contrast T1-weighted images (**a**) the tumor appears less heterogeneous with isointense signal intensities when compared to the gray matter (**a**, *arrow*). On axial (**b**), coronal (**c**), and sagittal (**d**) T1-weighted images after i.v. administration of gadolinium the tumor shows a moderate amount of regressive changes (**b**–**d**, *arrowhead*) with pronounced rim enhancement (**b**–**d**, *arrow*)

enhancing mural nodule rarely associated with peripheral edema. The tumor matrix is typically hypodense or isodense, occasionally with calcifications [2]. The tumor can also present more atypical signs than suspected for a benign tumor with inhomogeneous enhancement, with irregular, not well demarcated tumor margins or internal hemorrhage [3]. The diffusion-weighted sequence is very important and reflects the benign nature of this tumor without diffusion restriction compared to high-grade tumors with remarkable diffusion restriction. The higher apparent diffusion coefficient (ADC) values for PA with loose stroma compared to medulloblastomas or atypical teratoid/rhabdoid tumors with densely packed small cells reflects the histological difference between these tumors [4–7]. The solid tumor enhances intensely, although it is not a high-grade neoplasm. Perfusion-weighted imaging studies showed relative cerebral blood volume (rCBV) values lower than 1.7 compared to the normally appearing contralateral white matter due to contrast material extravasation into interstitial spaces (high leakage value). High-grade gliomas usually show an elevation of rCBV [4]. The cyst wall can be present with or without enhancement. Leptomeningeal metastases are rare but have lower impact on the clinical course compared to metastatic high-grade tumors. The results of MR spectroscopy should not be misinterpreted, as the metabolite pattern appears aggressive with elevated choline and lactate and decreased N-acetylaspartate [4].

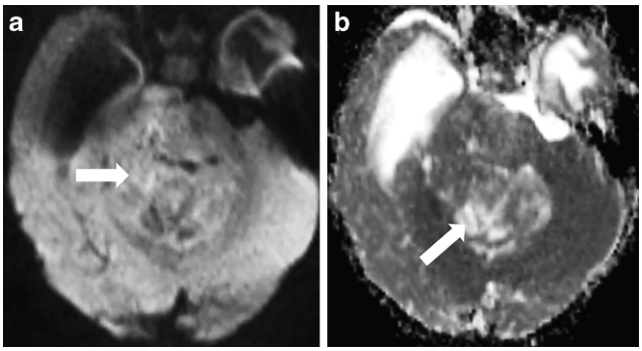

Fig. 3 On axial diffusion-weighted images the solid components of the lesion have an intermediate to high diffusion restriction on b 1000 images (**a**, *arrow*). The regressive changes within the lesion appear hyperintense on apparent diffusion coefficient (ADC) maps (**b**, *arrow*)

The pilomyxoid astrocytoma (PMA, WHO II) is a more aggressive myxoid variant of PA with higher risk of local recurrence and CSF dissemination. It is typical for infants and young children below 4 years. The mean age at onset is 18 months. Its appearance is similar to PA but is often more bulky/large and more frequently shows intratumoral hemorrhage. Calcification occurs but is uncommon. Of PMA 60% are supratentorially located but have also been reported in

the midbrain, cerebellum and 4th ventricle. This tumor does not show diffusion restriction [1, 8]. Given the young age, the location and intermediate to high diffusion restriction, a PA is improbable. A PMA is rare and fits well to the age of this patient. The tumor configuration and increased diffusivity of this case, however, is not typical for a PMA.

Medulloblastoma

The medulloblastoma (MB) is the most common brain tumor in infants accounting for nearly half of newly diagnosed brain tumors in children below 2 years of age. Approximately 10–15% of MBs are diagnosed within the first year of life. The tumor is more aggressive in the age group of children below 3 years and leptomeningeal dissemination at first diagnosis occurs more frequently in 27–43% of younger children [1]. The MB is not a single disease entity: four subgroups are classified with distinct genetic profiles, pathway signatures and clinicopathological features [1]. Infant MBs are present in the sonic hedgehog activated (SHH) group and group 3 commonly located in the midline with extension into the 4th ventricle. There is a predilection of the male gender of 1:2–4 [9, 10]. Calcifications are rarely seen (up to 20%). Occlusive hydrocephalus caused by the tumor is typical. An MB is generally hyperdense in native computed tomography (CT) and less hypointense in T2 than low-grade tumors due to an increased nuclear-cytoplasmic ratio (N/C ratio) of the tumor cells. It has remarkable diffusion restriction with high signal in the diffusion-weighted image and low signal on ADC maps. Measuring ADC values helps to differentiate tumors of the posterior fossa [6, 7]. The ADC values are significantly larger in PA than in ependymomas, which in turn demonstrated significantly larger ADC values than MBs [5]. Rodriguez Gutierrez et al. [11] used support vector machine-based classifiers using ADC histogram features and obtained very good discrimination among pediatric fossa tumor types (PA, ependymoma and MB). The degree of enhancement is variable and 11% do not enhance at all [12, 13]. The contrast uptake of secondary neoplasms may differ from the primary tumor. In contrast to other malignancies, metastases of MB tend to display a weaker enhancement than the primary tumor [14]. The diffusion sequence is very helpful to detect leptomeningeal spread and tumor recurrence especially if the tumor is not or less enhancing [15]. Compared to AT/RT (atypical teratoid/rhabdoid tumor) in MBs, hemorrhage is less common and more MBs were solid or predominantly solid tumors [16]. Usually the MB is a round mass in the 4th ventricle. In this case the tumor also showed a remarkable plastic extension into the outlets of the foramen of Luschka to the cerebellopontine angle cistern, atypical for a MB and typical for an ependymoma.

Atypical Teratoid/Rhabdoid Tumor

Atypical teratoid/rhabdoid tumor (AT/RT) is a rare malignant embryonal tumor in young children characterized by the presence of rhabdoid cells and with a predilection for the posterior fossa and supratentorial for the pineal region. Infratentorially it tends to occur off midline and grow into the cerebellopontine angle. It accounts for more than 20% of CNS tumors in infants. It is typically large and very heterogeneous with cysts, hemorrhage, calcifications and solid parts with high cellularity. Surgical resection is often limited by the large tumor with infiltrative growth pattern, the frequent involvement of multiple cranial nerves, vascular structures and brainstem. Approximately 20% already show CSF dissemination at the time of diagnosis [1, 16, 17]. The survival rate is poor with median survival around 17 months [18]. The ADC values of AT/RT are similar to those of MB [5, 16].

In the present case the tumor was heterogeneous but primarily solid with calcified and hemorrhage alterations. There were different areas of intermediate and high diffusion restriction. Inhomogeneous cystic changes were not in the foreground as would be expected for an AT/RT; however, due to the typical involvement of the cerebellopontine angle cistern and the very young age, the differential diagnosis (DD) of AT/RT must be considered.

Ependymoma

The ependymoma (EP; commonly WHO II) is a rare brain tumor arising from ependymal cells of the ventricle. The incidence is approximately 2 per million and two thirds of them are localized infratentorially. The median age at diagnosis ranges from 51 to 71 months and first presentation and diagnosis is below 3 years in 25–40% of the cases. A rare entity but the second most common type of EP is an anaplastic differentiation, WHO III [19, 20]. A peak incidence is reported at 1 year of age but it can occur at any age. There is no gender predilection [21].

The EPs are the second most common posterior fossa tumor in young children. In infants they are almost exclusively located infratentorially. About half of the EPs in the first year of life show the more aggressive anaplastic differentiation with poorer outcome [1]. The infratentorial EP is a lobulated mixed (solid and cystic) mass expanding and filling the 4th ventricle, causing obstructive hydrocephalus in 90% of cases. The tumor can typically extend through the outlet foramen: from the foramen of Luschka into the cerebellopontine angle cistern or from the foramen of Magendie in the cisterna magna dorsally along the upper cervical cord. This is highly specific but not entirely pathognomonic. The few MBs that extend through the 4th ventricular exit foramina show a more bulbous extension rather than thin tongues

of soft tissue through the foramina as in EPs [19, 22]. In the cisterns the tumor often insinuates surrounding structures and the encases the vessels and cranial nerves. Generally, the EPs show T1-hypointense and T2-hyperintense signals compared to brain parenchyma with inhomogeneous intratumoral signal. The solid tumor components usually show intense enhancement. Calcifications are detected in approximately half of the cases and hemorrhage in 10% by CT [23]. A minority of tumors show only little enhancement despite being predominantly soft tissue. Leptomeningeal spread is relatively rare ranging from 9% to 20% [19, 20]. Occurrence of subarachnoid spread is often detected at the time of disease recurrence and not initially [22].

Anaplastic EPs are larger and more aggressive, have a higher incidence of CSF dissemination, are inhomogeneous with cystic and hemorrhagic changes and more often associated with severe obstructive hydrocephalus [24]. Diffusivity of EPs is in general intermediate between that of PAs and MBs. As noted above, the ADC can help for the differentiation of cerebellar tumors in children [5]. In this case the tumor showed a typical appearance and location for an infratentorial EP but was relatively aggressive with calcifications, hemorrhages and neovascularization as demonstrated in the susceptibility weighted imaging (SWI) sequence (not shown), initially without any signs for leptomeningeal spread. Infiltration of the displaced brainstem by the extensive right-sided cisternal components and encasement of the vertebral and basilar arteries was shown. The tumor demonstrated different areas some with intermediate ADC values (areas of intermediate cellularity) and some with lower ADC values (areas of higher cellularity), indicating that it could be an EP with anaplastic differentiation in the first line. Other tumors with very high cellularity/diffusivity, namely AT/RT and MB, usually show very low ADC levels.

Histology

In the hematoxylin-eosin (H&E) stained sections of the formaldehyde-fixed and paraffin-embedded initial intraoperative biopsy material, a relatively pleomorphic neoplasm with regionally increased cellularity and necrosis was observed and classified as ependymoma (Fig. 4a). The following biopsy material yielded more tumor tissue which showed largely similar histomorphological features: the ependymal tumor displayed predominantly a solid growth pattern and appeared to be relatively sharply demarcated from few smaller fragments of the adjacent central nervous system (CNS) tissue. The tumor tissue harbored regional necrotic areas with some apoptotic cells (Fig. 4b). The tumor cells exhibited mostly small and round to oval-shaped chromatin dense nuclei with eosinophil cytoplasm whereas distinct tumor cell boundaries were partially not recognizable (Fig. 4a–c). Rarely, so called salt and pepper speckling of the chromatin was visible (Fig. 4a–c). Around small blood vessels a characteristic pattern of mostly monolayered pseudorosettes formed by radially arranged tumor cells with perivascular anuclear zones of glial fibrillary acid protein (GFAP)-rich, fibrillary processes was observed (Fig. 4a and 5a). Occasional dystrophic calcifications were seen locally in the present tissue as well as a few and mostly small acute hemorrhages, whereas hemosiderin deposits indicating older bleeding could not be detected (Fig. 4d). Besides many hyperchromatic nuclei, an increased abundance of mitotic figures was present (Fig. 4c). Accordingly, the proliferation index was increased and in total 10–15%, locally up to 20% of the tumor cells were marked in the Ki67/MIB1 immunohistochemical staining (Fig. 5b). Microvascular proliferation could be visualized in several regions by the Tibor-Pap silver staining (Fig. 4e). Marked desmoplastic components were absent in the present tissue.

Staining for GFAP was predominantly positive in the tumor tissue around the blood vessels (Fig. 5a). In addition, reactive astrogliosis was displayed by GFAP staining within the CNS tissue. Notably, staining against epithelial membrane antigen (EMA), which displays microlumina of tumor cells, uncovered a typical cytoplasmic dot-like and scarce ring-like positivity in some tumor cells (Fig. 5c). Within the ependymal tumor cells OLIG2 expression, indicative among others for gliomas, e. g. high-grade astrocytoma or oligodendroglioma [25], was absent (Fig. 5d). The neuronal markers Map2, synaptophysin and neuron specific enolase (NSE) were not expressed in the tumor tissue (not shown). Staining using a mutation-specific (R132H) antibody against isocitrate dehydrogenase 1 (IDH1) showed no specific reactions in the tumor cells (Fig. 5e).

Differential diagnoses for the current tumor include in general tumors of infants and young children e. g. PA, WHO grade I, or embryonal tumors such as medulloblastoma, WHO grade IV or AT/RT, WHO grade IV. Another rare differential diagnosis that may harbor some morphological similarities with ependymoma belongs to the recently defined group of embryonal tumors: C19MC-altered embryonal tumor with multilayered rosettes (ETMRs), WHO grade IV [26]. This newly defined entity also includes pediatric CNS embryonal tumors previously classified. as ependymoblastoma [27].

Regarding these differential diagnoses, (pseudo)rosettes are not a common feature of PA. Furthermore, the morphological features of medulloblastoma are quite distinct with small blue round tumor cells and neuroblastic Homer Wright rosettes. In contrast to the present tumor that displayed mainly monolayered pseudorosettes around blood vessels, ETMRs exhibit distinct true multilayered rosettes and form concentric cellular rings around nonvascular lu-

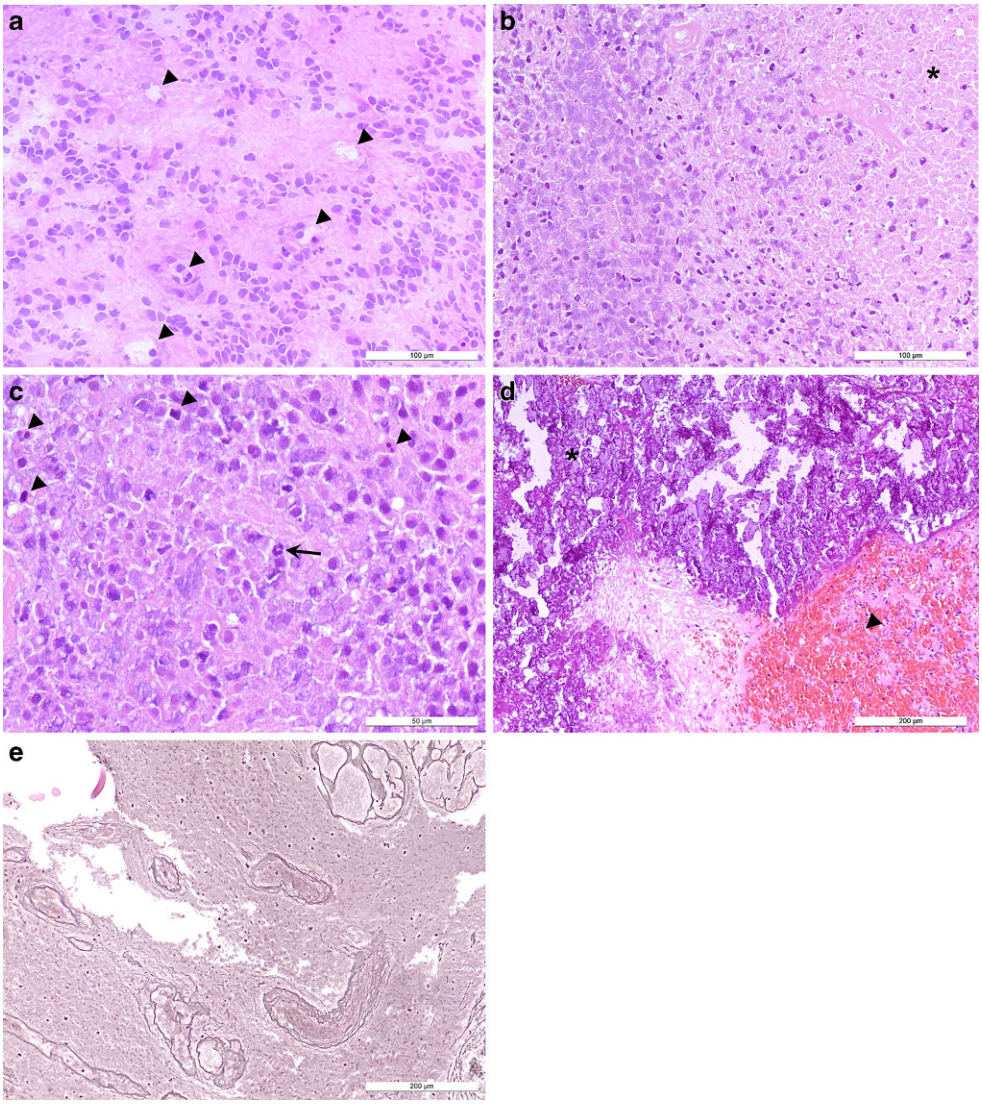

Fig. 4 Hematoxylin-eosin stained section of the intraoperative specimen (a–d) showing an ependymal tumor with pseudorosettes around small blood vessels (*arrowheads*, **a**) and regional necrosis (**b**, *asterisk*). Tumor cells feature round-oval, chromatin dense nuclei and mitotic (*arrowheads*) as well as apoptotic tumor cells are detectable (**c**, *arrow*). Dystrophic calcifications (**d**, *asterisk*) are present locally as well as a few and mostly small acute bleedings (**d**, *arrowhead*). Microvascular proliferation is visualized in various regions by Tibor-Pap silver staining (**e**). Size bars: **a**, **b** = 100 µm, **c** = 50 µm, **d**, **e** = 200 µm

mina. In addition, expression of markers, indicating neuronal differentiation (Map2, synaptophysin, NSE), was absent in the present specimen and opposed the diagnosis of embryonal tumors, such as medulloblastoma or ETMR. The highly malignant pediatric tumor AT/RT is reported to account for 10% of CNS tumors in young children [28]. In this case this differential diagnosis is ruled out by missing histomorphological hallmarks, such as rhabdoid-shaped tumor cells.

In summary, the histopathological finding of a glial, pleomorphic, relatively well-demarcated tumor with hypercellularity exhibiting characteristic perivascular pseudorosettes together with signs of anaplasia in terms of raised mitotic and proliferative activity as well as microvascular proliferation and geographic necrosis consequently leads to the diagnosis of anaplastic ependymoma, WHO grade III. The diagnosis of an ependymoma, WHO grade II, is not reasonable. The diagnosis was independently confirmed by the brain tumor reference center in Bonn, Germany.

Diagnosis

Anaplastic Ependymoma, WHO Grade III

Generally, ependymomas are tumors of children and adults and composed of neoplastic ependymal cells. Ependymal tumors comprise subependymoma (WHO grade I), myxopapillary ependymoma (WHO grade I), classical ependymoma (WHO grade II), anaplastic ependymoma (WHO grade III) and RELA-fusion positive ependymoma (WHO grade II–III) and are often located in the posterior fossa (about 60%) followed by supratentorial localization (30%) and in the spinal cord (10%); however, in infants and young children with an age less than 3 years 80% of

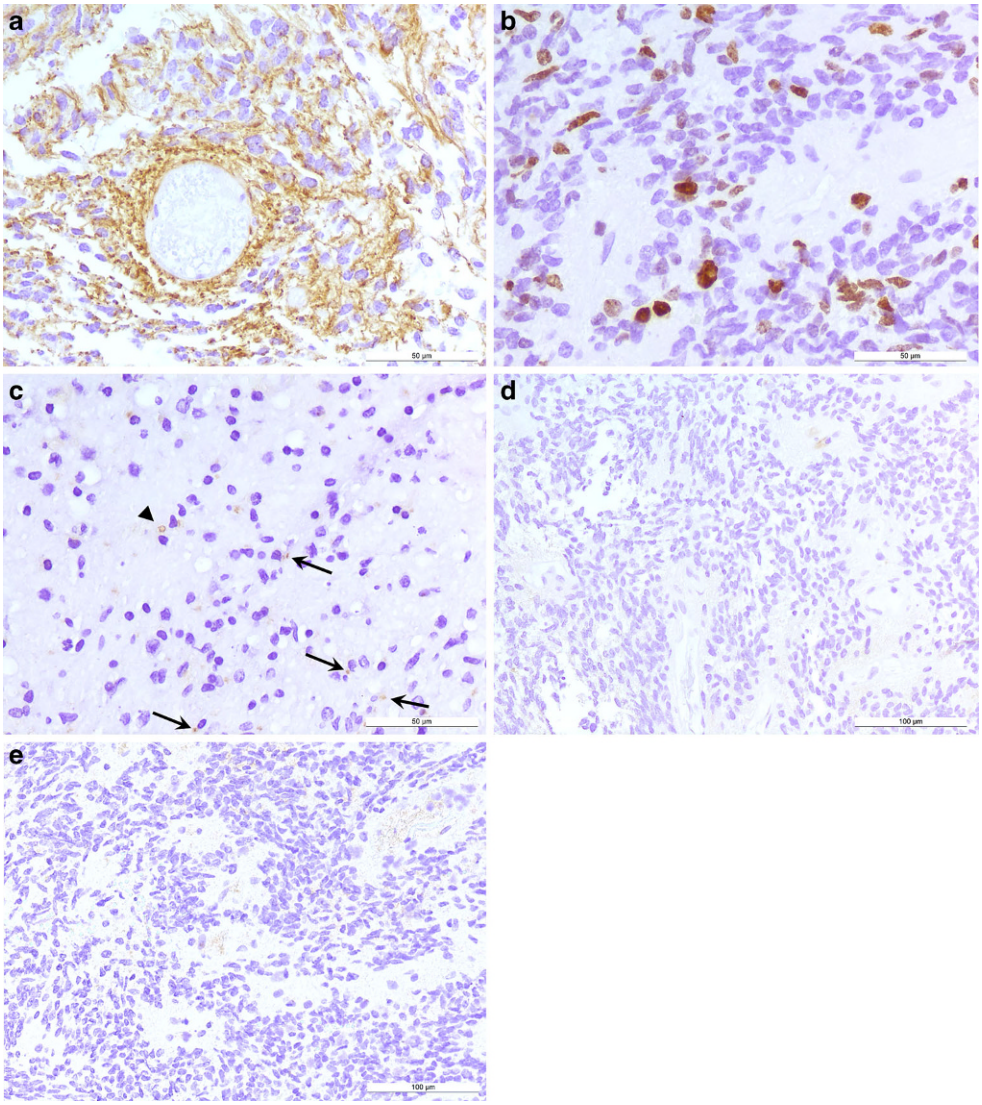

Fig. 5 Typical pseudorosettes with perivascular anuclear zones of GFAP-rich, fibrillary processes clearly shown by staining against GFAP (**a**). The proliferation index is locally highly increased tagging up to 20% of tumor cells, depicted by the MIB1 staining (**b**). Immunohistochemical staining against EMA reveals characteristic perinuclear dot-like (*arrows*) and ring-like (*arrowhead*) positivity in various tumor cells (**c**). The OLIG2 staining remains negative within the tumor tissue (**d**). Staining against IDH1-R132H, indicative for IDH-mutated astrocytomas and oligodendrogliomas [35] reveals no specific reaction in the present ependymal tumor (**e**). *Size bars*: **a**, **b** and **c** = 50 µm, **d**, **e** = 100 µm

ependymomas are found in the posterior fossa, demonstrating an age-matched spatial distribution of ependymomas [29]. Subependymomas are typically observed in adults and located in the ventricles whereas myxopapillary ependymoma are almost exclusively localized in the spinal cord (conus medullaris, cauda equine and filum terminale). Furthermore, in children ependymal tumors are the third most common type of CNS tumor after astrocytoma and medulloblastoma. They account for approximately 6–12% of all juvenile intracranial neoplasms and up to 30% in infants up to the age of 3 years [30, 31].

Histopathologically, three additional ependymoma variants can be distinguished: papillary, clear cell and tanycytic ependymoma; however, none of these features were detectable in the present specimen. By histological grading, ependymoma can be classified as low grade (WHO grade II) or anaplastic (WHO grade III) tumors according to the current WHO classification of CNS tumors [27], whereas an association between WHO grade, biological behavior and outcome is still unclear [32, 33]. More recently, molecular subgroups have been suggested as prognostic or predictive variables instead [27, 33, 34]. For example, the genetically defined RELA-fusion positive ependymoma which is often localized supratentorially is reported to have the worst outcome of all ependymal tumors [34].

Compliance with ethical guidelines

Conflict of interest C.A. Taschner, D. Erny, M.J. Shah, H. Urbach, U. Feige and M. Prinz declare that they have no competing interests.

Ethical standards All investigations described in this manuscript were carried out with the approval of the responsible ethics committee and in accordance with national law and the Helsinki Declaration of 1975 (in its current revised form). Informed consent was obtained from the patient in this case if identifiable from images or other information within the manuscript. In the case of the underage patient in this report, informed consent was obtained from the legal representatives.

References

1. Spennato P, Nicosia G, Quaglietta L, Donofrio V, Mirone G, Di Martino G, Guadagno E, del Basso de Caro ML, Cascone D, Cinalli G. Posterior fossa tumors in infants and neonates. Childs Nerv Syst. 2015;31:175–7.
2. Lee YY, Van Tassel P, Bruner JM, Moser RP, Share JC. Juvenile pilocytic astrocytomas: CT and MR characteristics. AJR Am J Roentgenol. 1989;152:1263–70.
3. Nakano Y, Yamamoto J, Takahashi M, Soejima Y, Akiba D, Kitagawa T, Ueta K, Miyaoka R, Umemura T, Nishizawa S. Pilocytic astrocytoma presenting with atypical features on magnetic resonance imaging. J Neuroradiol. 2015;42:278–82.
4. Gaudino S, Martucci M, Russo R, Visconti E, Gangemi E, D'Argento F, Verdolotti T, Lauriola L, Colosimo C. MR imaging of brain pilocytic astrocytoma: Beyond the stereotype of benign astrocytoma. Childs Nerv Syst. 2017;33:35–54.
5. Rumboldt Z, Camacho DL, Lake D, Welsh CT, Castillo M. Apparent diffusion coefficients for differentiation of cerebellar tumors in children. AJNR Am J Neuroradiol. 2006;27(6):1362–9.
6. Zitouni S, Koc G, Doganay S, Saracoglu S, Gumus KZ, Ciraci S, Coskun A, Unal E, Per H, Kurtsoy A, Kontas O. Apparent diffusion coefficient in differentiation of pediatric posterior fossa tumors. Jpn J Radiol. 2017;35:448–53.
7. Domínguez-Pinilla N, Martínez de Aragón A, Diéguez Tapias S, Toldos O, Hinojosa Bernal J, Rigal Andrés M, González-Granado LI. Evaluating the apparent diffusion coefficient in MRI studies as a means of determining paediatric brain tumour stages. Evaluación de la utilidad del coeficiente de difusión aparente en resonancia magnética para la diferenciación del grado tumoral de los tumores cerebrales pediátricos. Neurologia. 2016;31:459–65.
8. Alkonyi B, Nowak J, Gnekow A, Pietsch T, Warmuth-Metz M. Differential imaging characteristics and dissemination potential of pilomyxoid astrocytomas versus pilocytic astrocytomas. Neuroradiology. 2015;57:625–38.
9. Colafati GS, Voicu IP, Carducci C, Miele E, Carai A, Di Loreto S, Marrazzo A, Cacchione A, Cecinati V, Tornesello A, Mastronuzzi A. MRI features as a helpful tool to predict the molecular subgroups of medulloblastoma: State of the art. Ther Adv Neurol Disord. 2018;11:17–9.
10. Kline CN, Packer RJ, Hwang EI, Raleigh DR, Braunstein S, Raffel C, Bandopadhayay P1, Solomon DA1, Aboian M1, Cha S1, Mueller S1. Case-based review: Pediatric medulloblastoma. Neurooncol Pract. 2017;4:138–50.
11. Rodriguez Gutierrez D, Awwad A, Meijer L, Manita M, Jaspan T, Dineen RA, Grundy RG, Auer DP. Metrics and textural features of MRI diffusion to improve classification of pediatric posterior fossa tumors. AJNR Am J Neuroradiol. 2014;35:1009–15.
12. Erdem E, Zimmerman RA, Haselgrove JC, Bilaniuk LT, Hunter JV. Diffusion-weighted imaging and fluid attenuated inversion recovery imaging in the evaluation of primitive neuroectodermal tumors. Neuroradiology. 2001;43:927–33.
13. Rollins N, Mendelsohn D, Mulne A, Barton R, Diehl J, Reyes N, Sklar F. Recurrent medulloblastoma: Frequency of tumor enhancement on Gd-DTPA MR imaging. AJNR Am J Neuroradiol. 1990;11:583–7.
14. Bühring U, Strayle-Batra M, Freudenstein D, Scheel-Walter HG, Küker W. MRI features of primary, secondary and metastatic medulloblastoma. Eur Radiol. 2002;12:1342–8.
15. Aboian MS, Kline CN, Li Y, Solomon DA, Felton E, Banerjee A, Braunstein SE, Mueller S, Dillon WP, Cha S. Early detection of recurrent medulloblastoma: The critical role of diffusion-weighted imaging. Neurooncol Pract. 2018;5:234–40.
16. Koral K, Gargan L, Bowers DC, Gimi B, Timmons CF, Weprin B, Rollins NK. Imaging characteristics of atypical teratoid-rhabdoid tumor in children compared with medulloblastoma. AJR Am J Roentgenol. 2008;190:809–14.
17. Tekautz TM, Fuller CE, Blaney S, Fouladi M, Broniscer A, Merchant TE, Krasin M, Dalton J, Hale G, Kun LE, Wallace D, Gilbertson RJ, Gajjar A. Atypical teratoid/rhabdoid tumors (ATRT): Improved survival in children 3 years of age and older with radiation therapy and high-dose alkylator-based chemotherapy. J Clin Oncol. 2005;23:1491–9.
18. Ginn KF, Gajjar A. Atypical teratoid rhabdoid tumor: Current therapy and future directions. Front Oncol. 2012;2:114.
19. Zacharoulis S, Moreno L. Ependymoma: An update. J Child Neurol. 2009;24:1431–8.
20. Zacharoulis S, Ji L, Pollack IF, Duffner P, Geyer R, Grill J, Schild S, Jaing TH, Massimino M, Finlay J, Sposto R. Metastatic ependymoma: A multi-institutional retrospective analysis of prognostic factors. Pediatr Blood Cancer. 2008;50:231–5.
21. McKean-Cowdin R, Razavi P, Barrington-Trimis J, Baldwin RT, Asgharzadeh S, Cockburn M, Tihan T, Preston-Martin S. Trends in childhood brain tumor incidence, 1973–2009. J Neurooncol. 2013;115:153–60.
22. Barkovich AJ. Pediatric neuroimaging. Philadelphia: Lippincott Williams & Wilkins; 2005.
23. Swartz JD, Zimmerman RA, Bilaniuk LT. Computed tomography of intracranial ependymomas. Radiology. 1982;143:97–101.
24. Yuh EL, Barkovich AJ, Gupta N. Imaging of ependymomas: MRI and CT. Childs Nerv Syst. 2009;25:1203–13.
25. Otero JJ, Rowitch D, Vandenberg S. OLIG2 is differentially expressed in pediatric astrocytic and in ependymal neoplasms. J Neurooncol. 2011;104:423–38.
26. Spence T, Sin-Chan P, Picard D, Barszczyk M, Hoss K, Lu M, Kim SK, Ra YS, Nakamura H, Fangusaro J, Hwang E, Kiehna E, Toledano H, Wang Y, Shi Q, Johnston D, Michaud J, La Spina M, Buccoliero AM, Adamek D, Camelo-Piragua S, Peter Collins V, Jones C, Kabbara N, Jurdi N, Varlet P, Perry A, Scharnhorst D, Fan X, Muraszko KM, Eberhart CG, Ng HK, Gururangan S, Van Meter T, Remke M, Lafay-Cousin L, Chan JA, Sirachainan N, Pomeroy SL, Clifford SC, Gajjar A, Shago M, Halliday W, Taylor MD, Grundy R, Lau CC, Phillips J, Bouffet E, Dirks PB, Hawkins CE, Huang A. CNS-PNETs with C19MC amplification and/or LIN28 expression comprise a distinct histogenetic diagnostic and therapeutic entity. Acta Neuropathol. 2014;128:291–303.
27. Louis DN, Ohgaki H, Wiestler OD, Cavenee WK, editors. WHO classification of tumours of the central nervous system. Lyon: International Agency for Research on Cancer; 2016.
28. Biegel JA, Zhou JY, Rorke LB, Stenstrom C, Wainwright LM, Fogelgren B. Germ-line and acquired mutations of INI1 in atypical teratoid and rhabdoid tumors. Cancer Res. 1999;59:74–9.
29. Purdy E, Johnston DL, Bartels U, Fryer C, Carret AS, Crooks B, Eisenstat DD, Lafay-Cousin L, Larouche V, Wilson B, Zelcer S, Silva M, Bouffet E, Keene D, Strother DR. Ependymoma in children under the age of 3 years: A report from the Canadian Pediatric Brain Tumour Consortium. J Neurooncol. 2014;117:359–64.
30. Duncan J, Lows E Jr. Intracranial ependymomas. In: Kaye A, Lows E Jr, editors. Brain tumors. Edinburgh: Churchill Livingstone; 1995. pp. 493–504.
31. Taschner CA, Erny D, Shah MJ, Urbach H, Lutz K, Prinz M. Freiburg Neuropathology Case Conference: An infant with a supratentorial mass lesion. Clin Neuroradiol. 2015;25:211–7.
32. Ellison DW, Kocak M, Figarella-Branger D, Felice G, Catherine G, Pietsch T, Frappaz D, Massimino M, Grill J, Boyett JM, Grundy RG. Histopathological grading of pediatric ependymoma: Reproducibility and clinical relevance in European trial cohorts. J Negat Results Biomed. 2011;10:7.
33. Hubner JM, Kool M, Pfister SM, Pajtler KW. Epidemiology, molecular classification and WHO grading of ependymoma. J Neurosurg Sci. 2018;62:46–50.

34. Pajtler KW, Witt H, Sill M, Jones DT, Hovestadt V, Kratochwil F, Wani K, Tatevossian R, Punchihewa C, Johann P, Reimand J, Warnatz HJ, Ryzhova M, Mack S, Ramaswamy V, Capper D, Schweizer L, Sieber L, Wittmann A, Huang Z, van Sluis P, Volckmann R, Koster J, Versteeg R, Fults D, Toledano H, Avigad S, Hoffman LM, Donson AM, Foreman N, Hewer E, Zitterbart K, Gilbert M, Armstrong TS, Gupta N, Allen JC, Karajannis MA, Zagzag D, Hasselblatt M, Kulozik AE, Witt O, Collins VP, von Hoff K, Rutkowski S, Pietsch T, Bader G, Yaspo ML, von Deimling A, Lichter P, Taylor MD, Gilbertson R, Ellison DW, Aldape K, Korshunov A, Kool M, Pfister SM. Molecular classification of ependymal tumors across all CNS compartments, histopathological grades, and age groups. Cancer Cell. 2015;27:728–43.
35. Capper D, Weissert S, Balss J, Habel A, Meyer J, Jäger D, Ackermann U, Tessmer C, Korshunov A, Zentgraf H, Hartmann C, von Deimling A. Characterization of R132H mutation-specific IDH1 antibody binding in brain tumors. Brain Pathol. 2010;20:245–54.